Electronic Supplementary Material (ESI) for Soft Matter.

Supporting Information

Analysis of Network Formation and Long-Term Stability in Silica Nanoparticle Stabilized Emulsions

Maziar Derakhshandeh, Brandy K Pilapil, Ben Workman, Milana Trifkovic, Steven L Bryant**

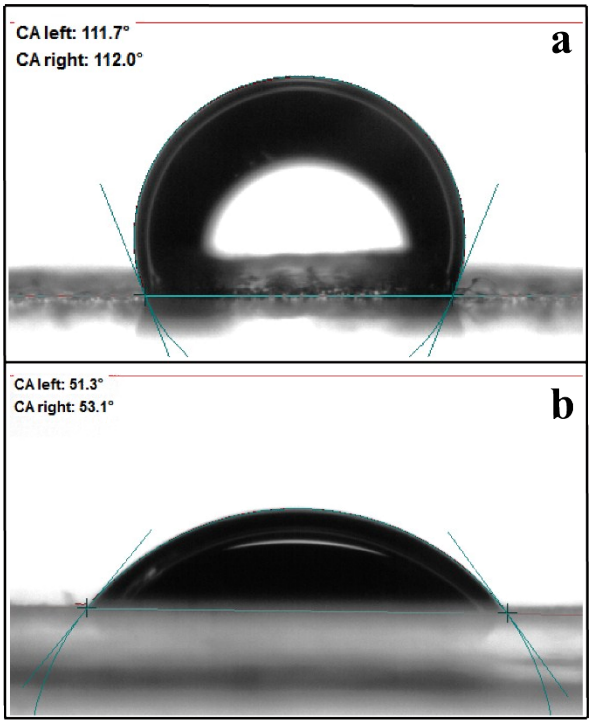

Figure S1. (a) Advancing contact angle of SNP-oil-water and (b) receding contact angle of SNP-dodecane-water.

Further Discussion of Contact Angle and Desorption Energy

It is shown that the polar and the disperse components of silica-air surface energies can be correlated with the percentage of unreacted Si-OH on the surface as[1,2]:

$$\gamma_s^d = 0.200(\%Si-OH) + 22.00 \quad \text{(S1)}$$

$$\gamma_s^p = 0.331(\%Si-OH) + 0.92 \quad \text{(S2)}$$

Where, γ_s^d and γ_s^p are disperse and polar components of silica-air surface energies, respectively. The percentage of Si-OH groups on the nanoparticles surface are obtained using the base titration procedure[3]. Furthermore, by using Owens and Wendt theory,[4] the interfacial tension between two different phases (a and b) can be obtained.

$$\gamma_a = \gamma_a^p + \gamma_a^b \tag{S3}$$

$$\gamma_{ab} = \gamma_a + \gamma_b - 2\sqrt{\gamma_a^p \gamma_b^p} - 2\sqrt{\gamma_a^d \gamma_b^d} \tag{S4}$$

Subsequently, the equilibrium three-phase contact angle (water-dodecane-NP) can be determined using Young equation[5].

$$\theta_{owp} = \cos^{-1}\frac{\gamma_{so} - \gamma_{sw}}{\gamma_{ow}} \tag{S5}$$

Where, γ_{ow} is dodecane-water interfacial tension, γ_{so} is silica-dodecane interfacial tension, and γ_{sw} is silica-water interfacial tension. The equilibrium three-phase contact angle is estimated using the surface energies and the percentage of unreacted Si-OH groups on the nanoparticles surface as 61°.

In addition to Equation S5, the equilibrium three-phase contact angle can also be determined from three-phase advancing and receding contact angles[6,7]. Water-dodecane contact angle measurements of NP-coated coverslips shown advancing and receding contact angles of 112°±10 and 52°±10 (obtained from 4 different droplets, Figure S9), respectively. The equilibrium three-phase contact angle can be obtained from advancing and receding contact angles as follow[6,7]:

$$\theta_{owp} = arccos\left(\frac{\Gamma_{adv} cos\theta_{adv} + \Gamma_{rec} cos\theta_{rec}}{\Gamma_{adv} + \Gamma_{rec}}\right) \tag{S6}$$

Where

$$\Gamma_{adv} = \left(\frac{sin^3\theta_{adv}}{2 - 3cos\theta_{adv} + cos^3\theta_{adv}}\right)^{1/3} \tag{S7}$$

$$\Gamma_{rec} = \left(\frac{sin^3\theta_{rec}}{2 - 3cos\theta_{rec} + cos^3\theta_{rec}} \right)^{1/3} \quad \text{(S8)}$$

The equilibrium three-phase contact angle is determined as 78±5° using the water/dodecane/HMDS-SNP advancing and receding contact angles. The Young equation neglects the effect of surface roughness on the equilibrium three-phase contact angle. Larger contact angle hysteresis induced by surface roughness[8] along with the inherent inaccuracy of equations used to estimate the surface energies from the extent of Si-OH coverage on the surface can explain the discrepancy observed (78° vs. 61°). The coverslips coated with untreated SNPs dispersed water droplets rapidly and thus three-phase contact angle could not be determined. The equilibrium hexadecane-water-silica contact angle for clean silica is reported to as ~13°.[9] Since surface tension of dodecane (i.e. 25.35 mN/m) is comparable to that of hexadecane (i.e. 27.47mN/m), a similar equilibrium three-phase contact angle is expected for dodecane-water-silica system. Surface treatment of SNPs is therefore predicted to increase the desorption energy of SNPs 400-fold (determined using equation 1), such that once SNPs are located at the interface, they able to pin to the oil-water interface and stabilize the oil droplets sterically.

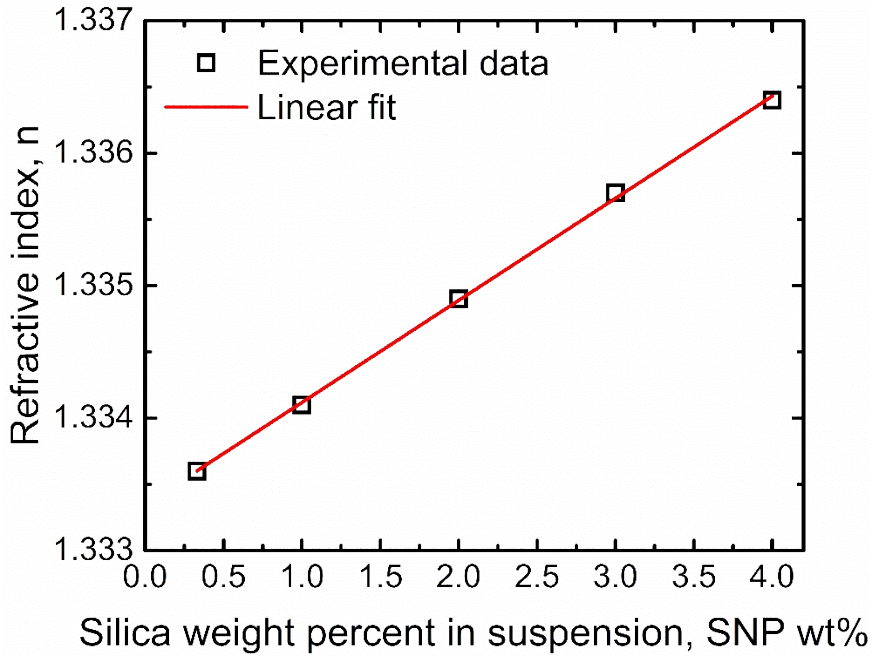

Figure S2. Plot of refractive indices as a function of silica weight fractions in initial suspensions. A linear relationship is observed allowing us to determine the nanoparticle loadings within emulsions.

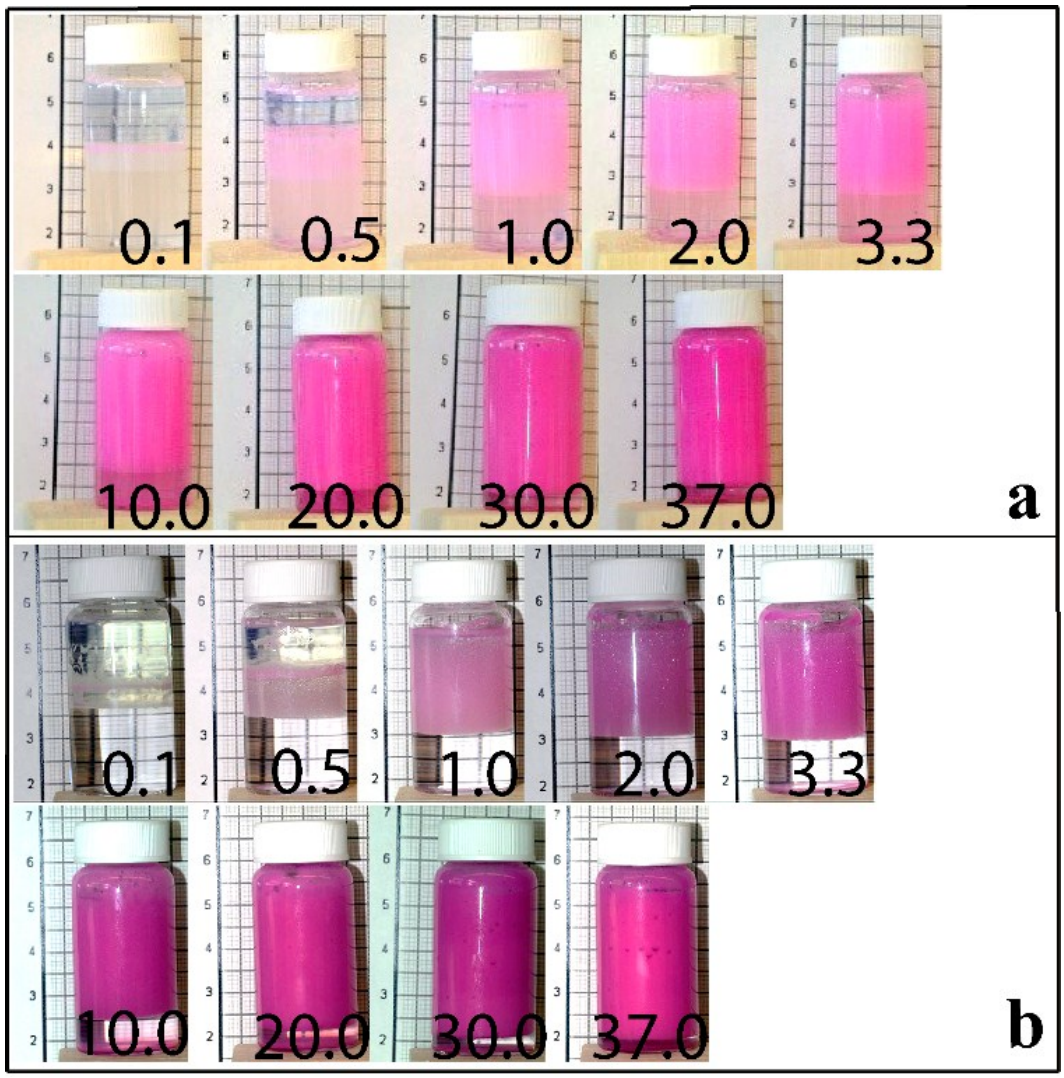

Figure S3. Vial images of emulsions prepared with different SNP concentrations after (a) 1 day and (b) 30 days of aging. For emulsions with 0.1 and 0.5 mg_{SNP}/mL_o, only a portion of the oil phase is emulsified and extensive coalescence due to partial coverage of their oil/water interface results in significant destabilization after 30 days (increase in droplet size, loss of oil from droplets to the excess oil phase layer). All other emulsions were found to be stable for the 30 days period based on vial images.

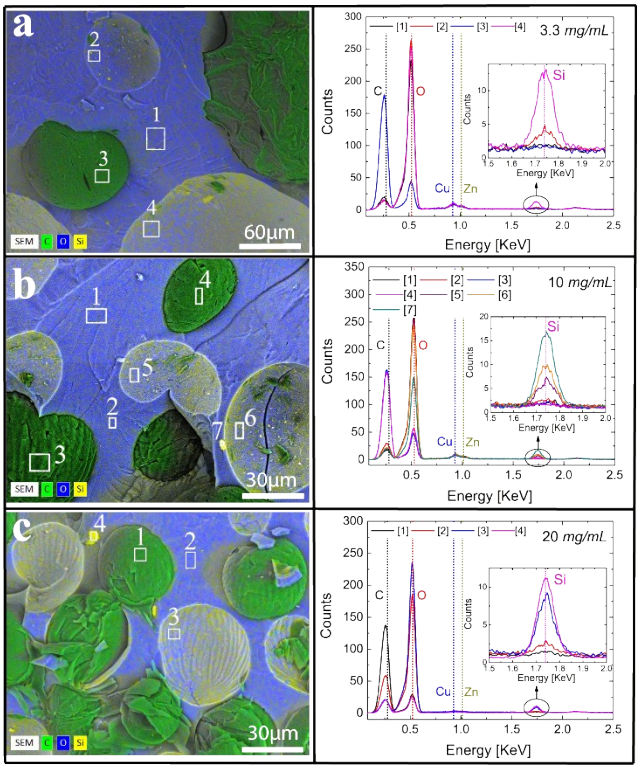

Figure S4. Left column; cryo-scanning electron microscopy images overlayed with energy dispersive X-ray spectroscopy (EDX) maps of silicon (yellow – indicating the presence of SNPs), oxygen (blue – indicating the water phase), and carbon (green – indicating the oil phase) for dodecane-in-water emulsions prepared with differing SNP concentrations of (a) 3.3 mg_{SNP}/mL_o, (b) 10.0 mg_{SNP}/mL_o, and c) 20.0 mg_{SNP}/mL_o. Right column: EDX spectrums of different regions as indicated on the images to their left. During cryo-SEM fracturing, droplets are either fractured in half (seen in green), or torn from the surface revealing relict droplet interfaces (seen as indentations in the water phase). The high concentration of silicon EDX signal (seen in regions a2, a4, b5, b6 and c3) at these relict interfaces confirms the interfacial adsorption of SNPs in the emulsions. When silicon is found in the excess water phase, it is generally associated to a SNP aggregate, such as in region c4.

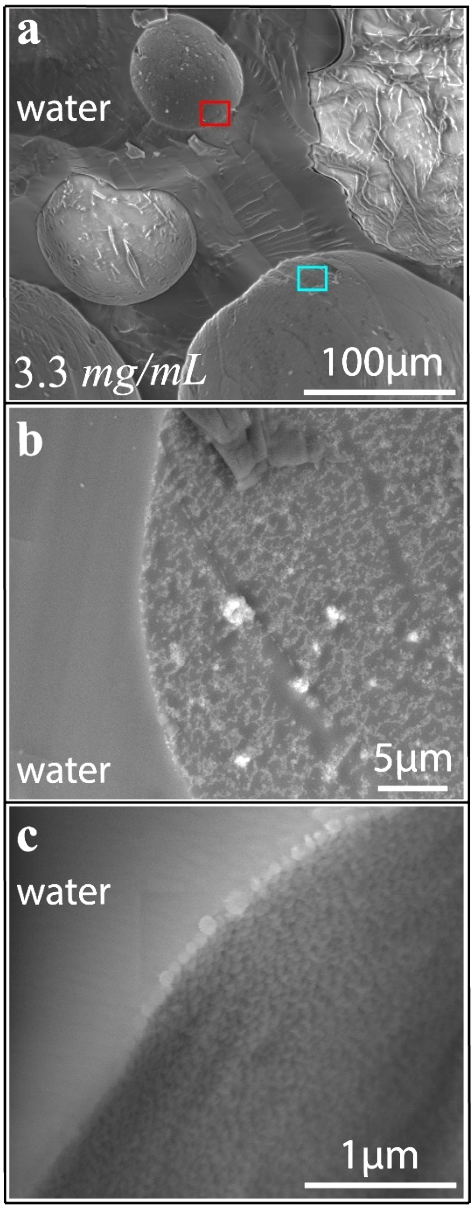

Figure S5. Cryo-SEM images obtained for a 3.3 mg_{SNP}/mL_o emulsion; (a) low magnification image showing the range in droplet sizes; (b) and (c) higher magnification images of the regions indicated in (a) with a red and blue box, respectively. Upon fracturing of the sample for cryo-SEM imaging, the oil droplets are torn from the surface, revealing "impressions" of oil droplets. While some droplets are found to be fully covered by SNPs (c), others are seen to have partial SNP coverage (b). These droplets can break and contribute to partial destabilization by prolong aging. The SEM image in (c) was also used to estimate the oil-water-particle contact angle.

Figure S6. Images of hand shaken emulsions obtained with ~5 wt % HMDS-SNPs dispersed in the water phase before (a) and after (b) the addition of 1 g of NaCl 1 day after preparation. It can be seen here that large droplets stabilized by the HMDS-SNPs are only observed in the presence of salt when such a low energy emulsification method is used, suggesting that electrostatic repulsion governs, in part, the formation of SNP stabilized emulsions.

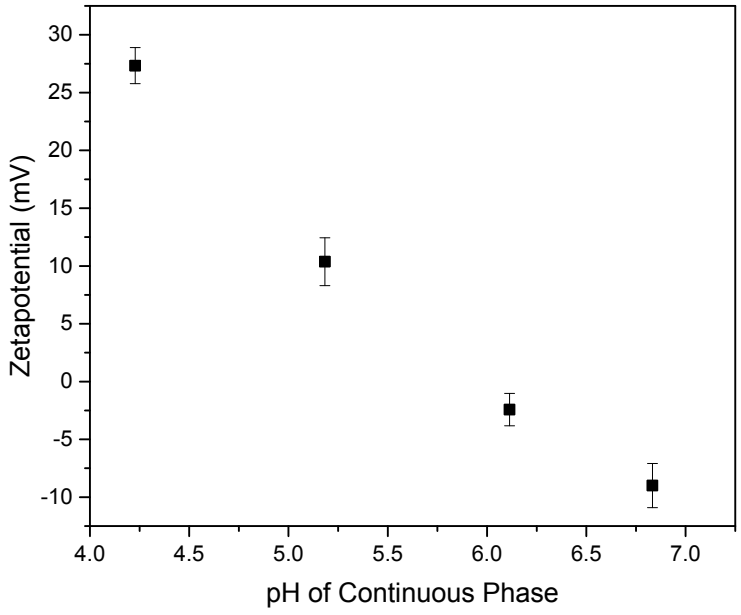

Figure S7. Results obtained from a zeta potential pH titration of SNP stabilized emulsion droplets (13 ± 2 μm diameter). The initial pH of the deionized water continuous phase is 6.8 ± 0.1 and is increased incrementally to the lowest value of 4.2 through the addition of 0.01 and/or 0.1 M HCl using a Malvern MPT-2 autotitrator. The sample was stirred using a magnetic stir bar throughout the experiment to ensure that the emulsion droplets remained dispersed and the effective mixing of titrant.

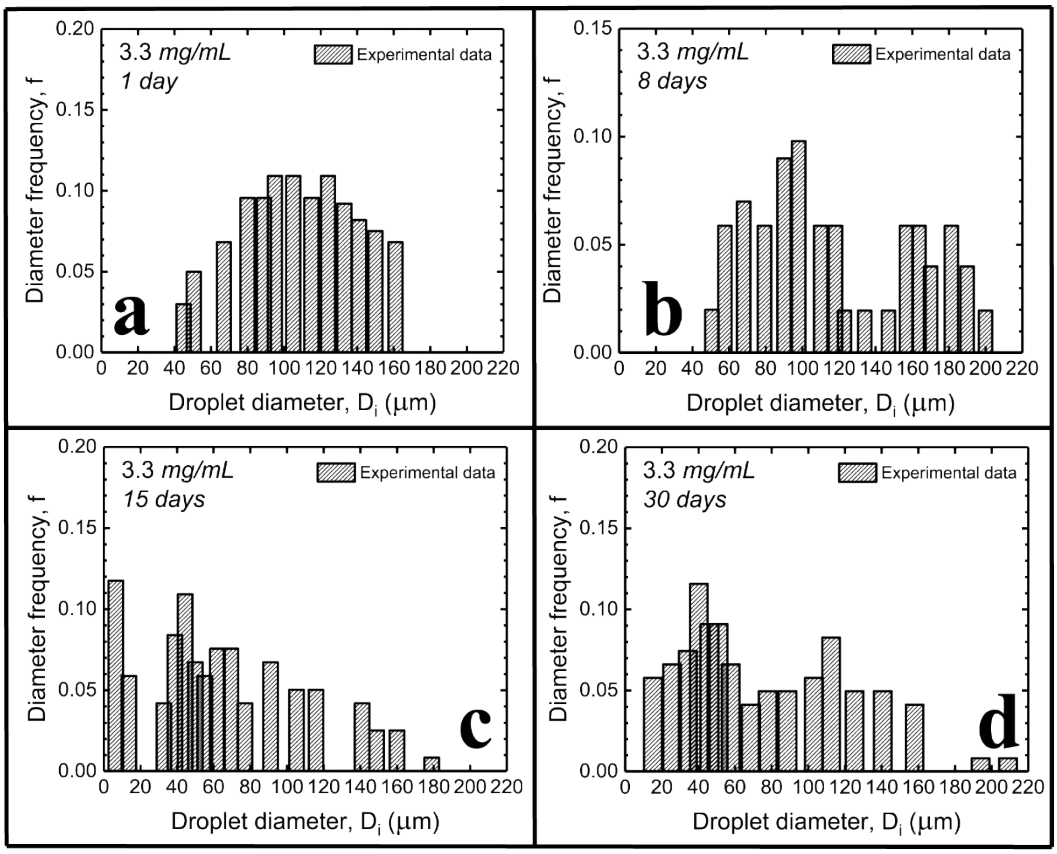

Figure S8. Droplet size distributions of emulsions made with M_{SNP}/V_o of 3.3 mg/mL after a) 1 day, b) 8 days, c) 15 days, and d) 30 days of aging. no clear trend is observed by aging, an indication of unstable emulsion.

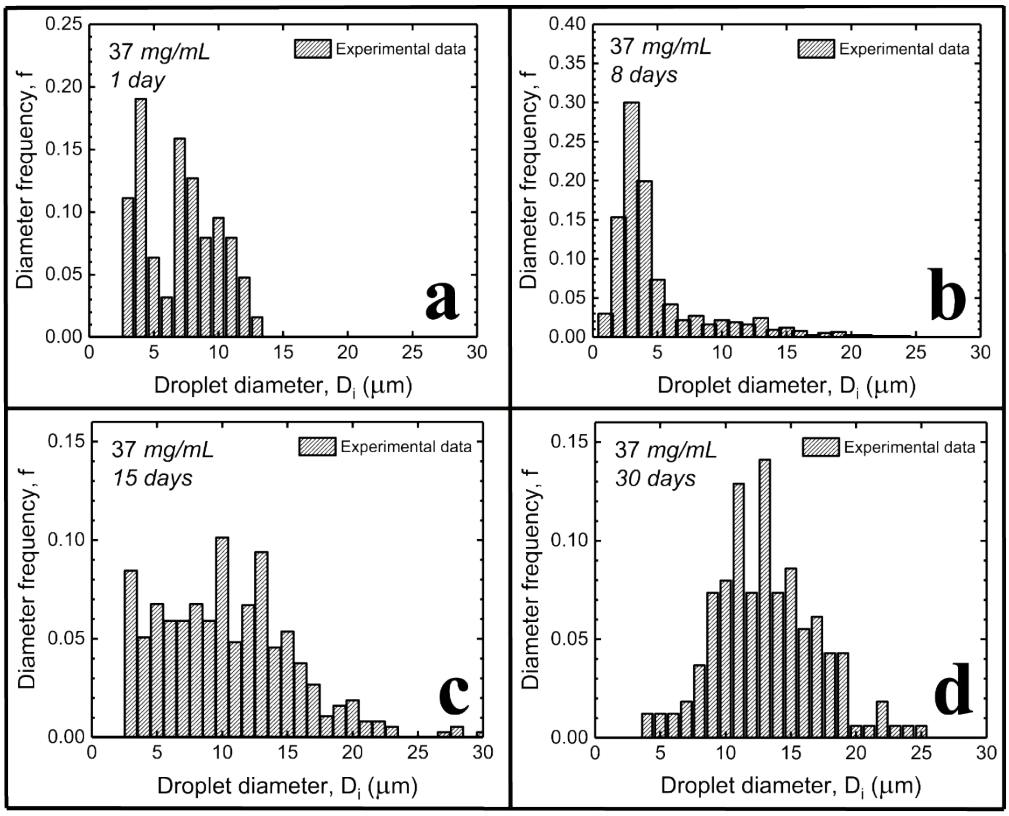

Figure S9. Droplet size distributions of emulsions made with $^{M_{SNP}}/_{V_o}$ of 37 mg/mL after a) 1 day, b) 8 days, c) 15 days, and d) 30 days of aging showing that slower droplet-droplet coalescence kinetics are observed in comparison with 10 and 20 mg/mL emulsions.

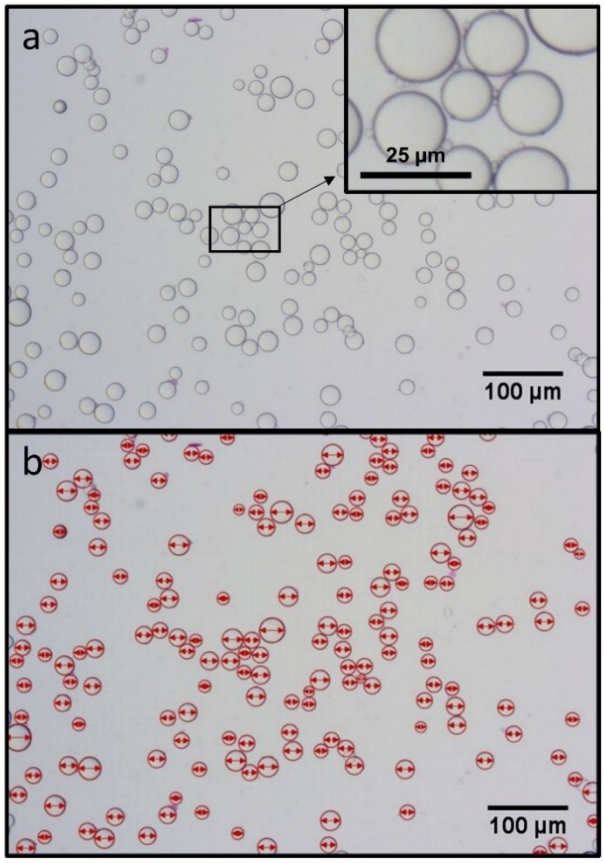

Figure S10. (a) Example of optical microscope image used in the determination of droplet size and size distribution. (b) Example of droplet measurement markup for the image in (a). Note that evidence of small droplets (< 3 µm) is present, e.g. in between larger droplets in the inset of (a), but their measurement was not pursued owing to the high error in this measurement.

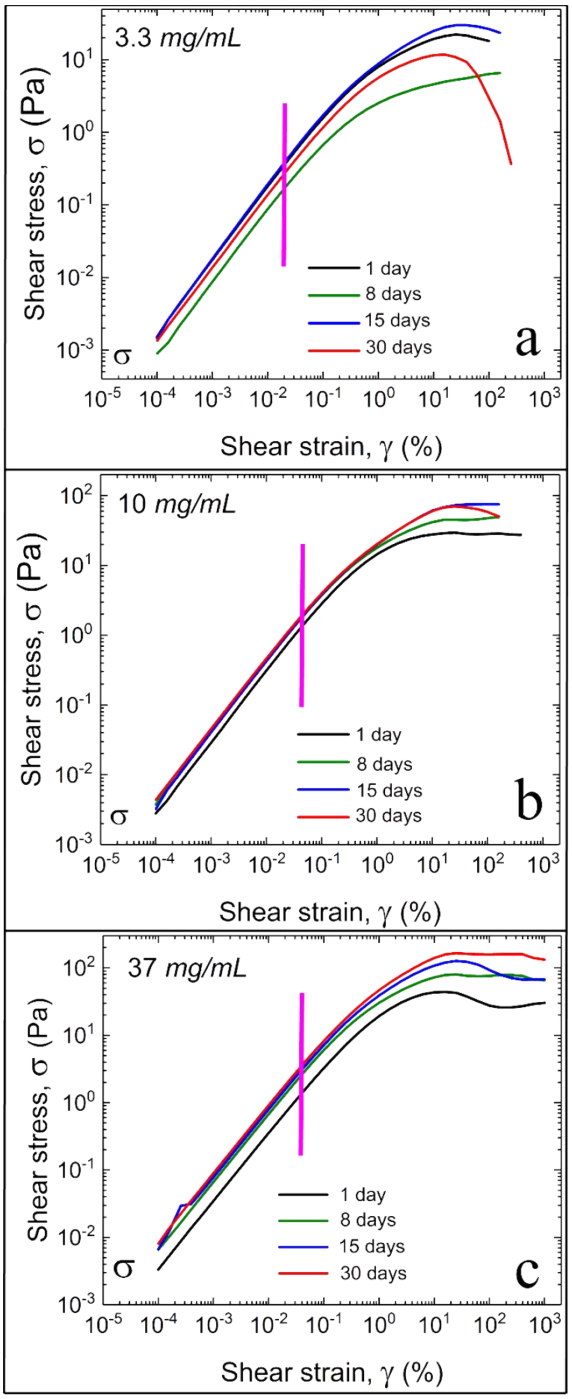

Figure S11. Shear stress vs. shear strain for (a) 3.3 mg/mL emulsion, (b) 10 mg/mL emulsion and (c) 37 mg/mL emulsion. Magenta vertical line on each graph depicts the limit of linear viscoelastic envelope (LVE).

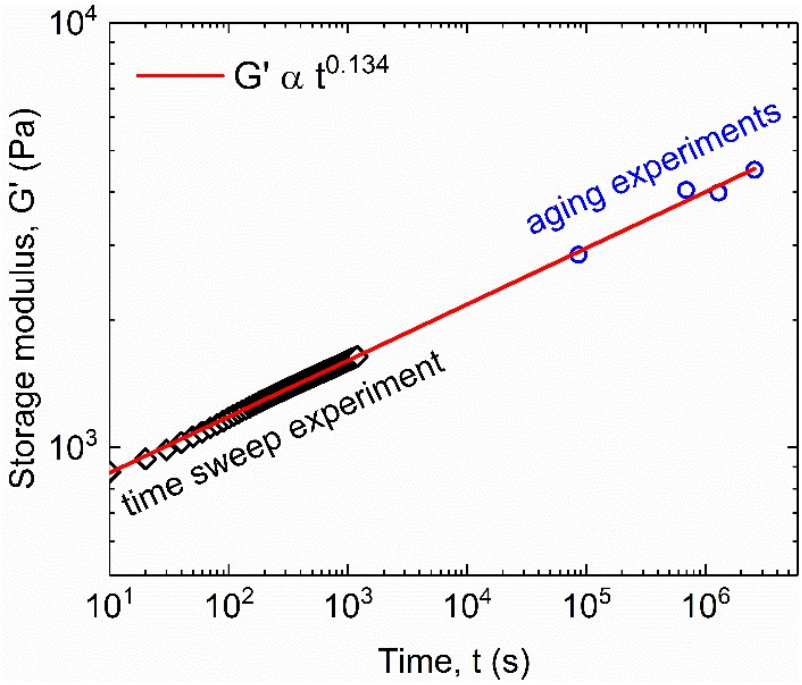

Figure S12. Growth of the storage modulus G' with time for emulsions prepared with 10 mg_{SNP}/mL_o. A time sweep experiment was performed on the 10 mg_{SNP}/mL_o emulsion sample after pre-shearing at the crossover strain for 90 seconds to break any network formed previously. Aging experiment data shown here is derived from that seen in Figure 5.

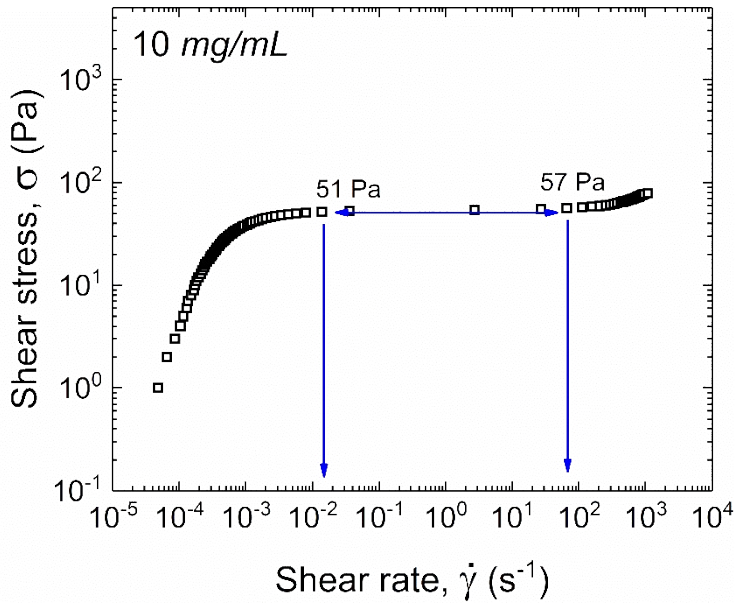

Figure S13. Transient flow curve of 10 mg_{SNP}/mL_o emulsion after 7 days of aging obtained under stress-controlled condition. A plateau in the flow curve is observed for shear stresses between 51 and 57 Pa indicating the shear banding instability.

Further Analysis of Network Formation Behavior:

In 2005, Manley et al.[1] studied the aging behavior of silica colloid gels to elucidate the time-dependent behavior of these materials. This work shows that the storage modulus increased with time over 13 hours, and the behavior was generally attributed to hydrogen bonding between free silanol groups on the surfaces of the silica colloids. Manley et al. reported an increase in in storage modulus proportional to time$^{0.4}$.[10] In our work, an exponent of ~0.13 was obtained and captured well by both time sweep experiment and storage modulus of samples after 1, 8, 15 and 30 days of aging. We suggest that the discrepancy in these relations (lower exponent value) arise from the electrostatic repulsion between species in our system, as Manley et al. added $MgCl_2$ salt to their colloidal gels as to minimize electrostatic contributions, as well as the adsorption of organic solvent molecules to the SNP surfaces, as discussed in the context of zetapotential analysis in the main text.

Surface Coverage Comparison: Laser Scanning Confocal Microscopy versus Coverage Based on Sauter Average Droplet Diameter Analysis:

A surface coverage of 92 ± 4 % was determined based on image analysis of LSCM 3D images. Since the resolution of the LSCM is greater than the SNP diameter, any regions of close-packed SNPs at the interface appear as 100% coverage. In order to compare this surface coverage to that of the theoretically obtained value of 77% (based on the concentration of SNPs incorporated into the creamed emulsion phase and the Sauter average droplet diameter), the resolution limitations of the LSCM images must be accounted for. Assuming that the SNPs are monodisperse and hexagonally close-packed at the interfaces (based on cryo-SEM data) and that the interface is flat in relation to the SNPs (based on the order of magnitude difference in diameters between SNPs

and emulsion droplets), multiplying the LSCM determined surface coverage by the theoretical surface coverage of close-packed circles (90.69%) provides a realistic estimate of the SNP droplet surface coverage of ~ 83 %. This value is slightly overestimated, considering that the SNPs due not pack consistently at a density of 90.69% due to deviations in the SNP particle size upon synthesis and the presence of SNP aggregates. Nonetheless, these values agree well within reasonable error, supporting the conclusion that the "holes" in the surface coverage are consistent with even the theoretical calculation of surface coverage.


SI video.mp4

Video S1. High-frame-rate confocal imaging of 20mg/mL emulsions showing SNPs are jammed at the oil-water interface (no observable motion) while the minimal SNPs within the continuous phase are moving due to their Brownian motion.

References:

1 B. P. Binks and J. H. Clint, *Langmuir*, 2002, **18**, 1270–1273.

2 B. P. Binks, A. K. F. Dyab and P. D. I. Fletcher, *Phys. Chem. Chem. Phys.*, 2007, **9**, 6391–6397.

3 G. W. Sears, *Anal. Chem.*, 1956, **28**, 1981–1983.

4 D. K. Owens and R. C. Wendt, *J. Appl. Polym. Sci.*, 1969, **13**, 1741–1747.

5 T. Young and others, *Philos. Trans. R. Soc. London*, 1805, **95**, 65–87.

6 R. Tadmor, *Langmuir*, 2004, **20**, 7659–7664.

7 E. Chibowski and K. Terpilowski, *J. Colloid Interface Sci.*, 2008, **319**, 505–513.

8 Y. C. Jung and B. Bhushan, *J. Microsc.*, 2008, **229**, 127–140.

9 J. W. Grate, K. J. Dehoff, M. G. Warner, J. W. Pittman, T. W. Wietsma, C. Zhang and M.

Oostrom, *Langmuir*, 2012, **28**, 7182–7188.

10 S. Manley, B. Davidovitch, N. R. Davies, L. Cipelletti, A. E. Bailey, R. J. Christianson, U. Gasser, V. Prasad, P. N. Segre, M. P. Doherty and others, *Phys. Rev. Lett.*, 2005, **95**, 48302.